Measuring Magnetic Fields with Magnetic-Field-Insensitive Transitions

Yotam Shapira,* Yehonatan Dallal, Roee Ozeri, and Ady Stern
Department of Physics, Weizmann Institute of Science, Rehovot 7610001, Israel

(Received 19 February 2019; published 27 September 2019)

Atomic sensing is, at large, based on measuring energy differences. Specifically, magnetometry is typically performed by using a superposition of two quantum states, the energy difference of which depends linearly on the magnetic field due to the Zeeman effect. The magnetic field is then evaluated from repeated measurements of the accumulated dynamic phase between the two Zeeman states. Here we show that atomic clock states, with an energy separation that is independent of the magnetic field, can nevertheless acquire a phase that is magnetic field dependent. We experimentally demonstrate this on an ensemble of optically trapped ^{87}Rb atoms. Finally, we use this effect to propose a magnetic field sensing method for static and time-dependent magnetic fields and analyze its sensitivity, showing it essentially allows for high-sensitivity magnetometery.

DOI: 10.1103/PhysRevLett.123.133204

Magnetometry is widely used in many diverse fields [1–8]. Atomic magnetometry is performed by tracking an accumulated dynamical phase of a magnetic-field-dependent transition of choice, which evolves due to Larmor precession, and comparing it to a stable local oscillator, e.g., the Zeeman ground state manifold of ^{87}Rb atoms compared to a driving rf field. Such a system was originally proposed by Dehmelt [9] and demonstrated by Bell and Bloom [10,11]. Measuring an accumulating dynamical phase is a prevalent approach of atomic sensing [12,13].

Similarly, atomic clocks operate by locking a local oscillator, an optical or rf source, to a transition frequency between two quantum states. Since stability is a crucial property of the clock, the atomic states are chosen such that their transition is as insensitive as possible to ambient magnetic fields [14,15]. The dependence of the transition between such *clock states* on magnetic fields typically vanishes at first order. For example, the $|6^2S_{1/2}, F = 4, m_F = 0\rangle \leftrightarrow |6^2S_{1/2}, F = 3, m_F = 0\rangle$ transition in the ^{133}Cs atom, on which the International System of Units (SI) second is defined [16].

Here we investigate atomic clock states and show, theoretically and experimentally, that a magnetic-field-dependent phase difference between two atomic states can arise, even when the transition energy does not depend on the magnetic field. Our approach generalizes the topological π phase shift acquired by $m = 0$ atomic states, upon flipping the magnetic field direction, which was discovered by Robbins and Berry [17]. By driving the clock states appropriately, this phase is no longer discrete; rather it becomes continuous and indicative of the magnetic field direction.

The clock states differ by their symmetry under rotations and have a constant energy difference, e.g., the hyperfine splitting. In a frame rotating with an on-resonance drive, the states become degenerate, but their symmetry difference is translated to a dependence of the coupling on the direction of the magnetic field.

We utilize this effect by mapping rotations of the magnetic field to its magnitude, and propose a clock-state-based magnetometry method. We explore the method's sensitivity, and show that it allows for high-sensitivity magnetometry. Furthermore, we discuss the relevance of this effect to the performance of atomic clocks.

Our derivations below are general for atomic clock states; however, for simplicity we consider the $|1,0\rangle \equiv |F = 1, m_F = 0\rangle$ and $|2,0\rangle$ clock states of the $5S_{1/2}$ ground level of ^{87}Rb, with a transition energy that is in leading order magnetic field independent.

We begin by deriving the Breit-Rabi Hamiltonian in the clock $m_F = 0$ subspace [18], with an additional driving term. The lab-frame Hamiltonian of the $5S_{1/2}$ ground level of ^{87}Rb is given by

$$\begin{aligned} H &= H_{\mathrm{hf}} + H_Z + V(t), \\ H_{\mathrm{hf}} &= \frac{\hbar A_{\mathrm{hf}}}{2} \boldsymbol{I}\cdot\boldsymbol{J}, \\ H_Z &= \mu_N g_I \boldsymbol{B}\cdot\boldsymbol{I} + \mu_B g_J \boldsymbol{B}\cdot\boldsymbol{J}, \\ V &= \frac{\hbar}{\mu}\left(\frac{\boldsymbol{\Omega}}{2} e^{i\omega_{\mathrm{rf}} t} + \mathrm{H.c.}\right)\cdot(\mu_N g_I \boldsymbol{I} + \mu_B g_J \boldsymbol{J}), \end{aligned} \tag{1}$$

where H_{hf} is the hyperfine interaction Hamiltonian, which couples the nucleus spin operators $\boldsymbol{I}$ with the electronic spin operators $\boldsymbol{J}$, such that the hyperfine splitting is A_{hf}. The term H_Z is the Zeeman Hamiltonian, describing the coupling of the quantization magnetic field, $\boldsymbol{B} = B\hat{b}$, to the nuclear and electronic spins through their respective Bohr magnetons, μ_N and μ_B, and the Landé g factors, g_I and

 © 2019 American Physical Society

g_J. The term V describes the same Zeeman coupling to an additional time-dependent, rf, magnetic field used to drive transitions between the two clock states. We assume that $\mathbf{\Omega}$ is complex, i.e., that the rf drive can be written as two orthogonal quadratures. For simplicity we restrict $\mathbf{\Omega}$ such that the resulting polarization ellipse lies in a plane containing the quantization field direction. Furthermore, we have defined $\mu \equiv \mu_N g_I - \mu_B g_J$.

The hyperfine Hamiltonian in Eq. (1) can be diagonalized in the $|F, m_F\rangle$ basis, with F the total angular momentum and m_F its projection along the quantization magnetic field direction $\hat{b}$. By shifting it appropriately it becomes $H_{\rm hf} = (\hbar A_{\rm hf}/2)(\delta_{F,2} - \delta_{F,1})$. In this basis, H_Z can be written as a direct sum of five subspaces marked by their m_F values: $H_Z = H_Z^{m_F=-2} \oplus H_Z^{m_F=-1} \oplus \cdots \oplus H_Z^{m_F=2}$. In the clock subspace the Zeeman Hamiltonian is $H_Z^{m_F=0} = (\mu B/2)\tau^x$, such that $\boldsymbol{\tau} = (\tau^x, \tau^y, \tau^z)$ are Pauli spin operators acting in the clock subspace.

When $\omega_{\rm rf}$ is tuned close to the clock transition frequency and far detuned from all other transitions (compared to $|\mathbf{\Omega}|$), we can assume it does not excite any transitions outside of the clock subspace.

The lab-frame Hamiltonian in the clock subspace is therefore composed of the hyperfine splitting, a Zeeman term, and the rf drive:

$$H_{\rm clk,lab} = \frac{\hbar A_{\rm hf}}{2}\tau^z + \frac{1}{2}[\mu B + \hbar(\mathbf{\Omega}\cdot\hat{b}e^{i\omega_{\rm rf}t} + \text{H.c.})]\tau^x. \quad (2)$$

In the absence of the rf drive, the B-dependent Zeeman term weakly mixes the $|2,0\rangle$ and $|1,0\rangle$ states, resulting in a small energy shift, which is quadratic in the Breit-Rabi parameter, $(\mu B/\hbar)/A_{\rm hf}$, and is known as the second-order Zeeman shift. In leading order the $m_F = 0$ states are clock states. For ^{87}Rb the ground state hyperfine frequency splitting is approximately 6.8 GHz while the Zeeman splitting in these manifolds is approximately $\pm\Delta m \times 0.70$ MHz/G [19]; thus we may neglect this term for a wide range of magnetic field magnitudes.

We change to a frame rotating with $(\hbar\omega_{\rm rf}/2)\tau^z$, and perform a rotating wave approximation, neglecting terms rotating with rate $\geq \omega_{\rm rf}$, to obtain the interaction Hamiltonian,

$$H_{{\rm clk},I} = \left(\frac{\hbar\eta}{2}\right)\tau^z + \frac{\hbar}{2}(\mathbf{\Omega}\cdot\hat{b}\tau^+ + \text{H.c.}), \quad (3)$$

with the rf drive detuning, $\eta = A_{\rm hf} - \omega_{\rm rf}$. Equation (3) shows that the phase of the Rabi frequency is sensitive to the projection of the rf field on the magnetic field direction.

For an elliptically polarized rf field, $\mathbf{\Omega} = e^{i\theta}(\mathbf{\Omega}_1 + i\mathbf{\Omega}_2)$, where $\mathbf{\Omega}_1$ and $\mathbf{\Omega}_2$ are the major and minor orthogonal axes of the polarization ellipse and θ is the rf phase, the on-resonance Hamiltonian is

$$\begin{aligned} H_{\rm clk} &= \frac{\hbar}{2}\Omega_{\rm eff}[\cos(\xi)\tau^x + \sin(\xi)\tau^y], \\ \Omega_{\rm eff} &= \sqrt{(\mathbf{\Omega}_1\cdot\hat{b})^2 + (\mathbf{\Omega}_2\cdot\hat{b})^2}, \\ \xi &= \theta + \arctan\left(\frac{\mathbf{\Omega}_2\cdot\hat{b}}{\mathbf{\Omega}_1\cdot\hat{b}}\right), \end{aligned} \quad (4)$$

where we have arbitrarily defined τ^x as the rotation operator acting at $\theta = 0$. Equation (4) gives rise to a Ramsey-like Hamiltonian where ξ plays the role of the pulse phase; i.e., it is the angle between the $\hat{x}$ axis and the Rabi vector on the equator of the Bloch sphere spanned by the two clock states.

We first show that the Hamiltonian in Eq. (4) generates Rabi nutation of population between the two clock states. Here, $\hat{b}$ lies in the polarization plane at an angle ϕ with $\mathbf{\Omega}_1$. This simplifies Eq. (4) such that $\xi = \theta + \phi$. The probability for the system to remain in the $|2,0\rangle$ state P_2 is

$$\begin{aligned} P_2 &= \sin^2\left(\frac{\Omega_1 T}{2}\beta\right), \\ \beta &\equiv \sqrt{\cos^2(\phi) + \tilde{\Omega}^2\sin^2(\phi)}, \\ \tilde{\Omega} &= \Omega_2/\Omega_1. \end{aligned} \quad (5)$$

As expected from a single pulse measurement, Eq. (5) is independent of the rf phase θ.

We experimentally demonstrate our methods on a cloud of ultracold ^{87}Rb atoms. The atoms are evaporatively cooled to $\approx$30 μK in a CO_2 laser quasielectrostatic trap. We drive the transition between the $F = 1$ and $F = 2$ hyperfine manifolds using a microwave antenna, tuned to the resonance frequency of this transition. The atoms are prepared in the $|1,0\rangle$ state using optical-pumping pulses on the $|F = 1\rangle \rightarrow |F = 2\rangle$ D_2 transition combined with microwave pulses. The population in the $|2,0\rangle$ state is measured using absorption imaging of the $|2,0\rangle$ state normalized by imaging of the atoms in both the $F = 1$ and $F = 2$ manifolds. Further information regarding the setup may be found in Refs. [20,21].

Figure 1(a) shows measured Rabi oscillations between the clock states, for varying pulse duration T and magnetic field angle ϕ. Our data are in good agreement with the model in Eq. (5) shown in Fig. 1(b).

The clock subspace Hamiltonian in Eq. (4) shows that the Rabi vector direction, i.e., the clock states' rotation axis, is determined by the orientation of the magnetic field with respect to the rf field polarization ellipse. It is the starting point for obtaining a magnetic-dependent phase shift between the two clock states.

We first show that a rotation of the magnetic field direction imprints a population difference on the two clock states. Our scheme consists of an on-resonance rf pulse, an adiabatic rotation of the quantization magnetic field by an

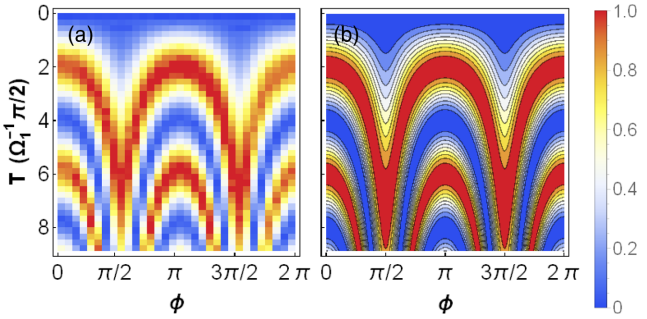

FIG. 1. Rabi oscillations between the clock states for varying pulse duration and magnetic field angles. Color indicates population in $|1,0\rangle$. (a) Data obtained by driving an ensemble of ^{87}Rb atoms with a rf drive, on resonance with the $|2,0\rangle \leftrightarrow |1,0\rangle$ transition. (b) Model according to Eq. (5), with $\tilde{\Omega} = 0.27$ in order to fit the data.

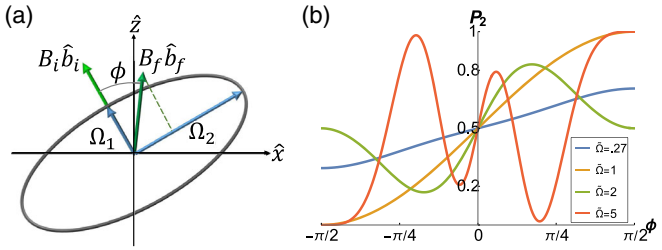

FIG. 2. Clock state population difference due to a magnetic field rotation. (a) Scheme layout. The polarization ellipse (gray) is aligned such that the major axis $\mathbf{\Omega}_1$ is parallel to the magnetic field direction $\hat{b}_i$ (green). The magnetic field is rotated on the polarization plane to $\hat{b}_f$, by an angle ϕ (dark green). For the rf phase, $\theta = (\pi/2)$, the $|2,0\rangle$ population is determined by the projection of the rotated magnetic field on Ω_2 (dashed green). (b) Population in the $|2,0\rangle$ state P_2 as a function of ϕ, according to Eq. (6), with $\theta = (\pi/2)$. As $\tilde{\Omega}$ grows, the sensitivity increases, seen as a larger slope, while the measurement range decreases due to the decreased separation between the two extrema around $\phi = 0$.

angle ϕ, and an additional on-resonance pulse, after which the clock state populations reflect the magnitude of ϕ.

We use an elliptic polarization of the rf driving field, such that the ellipse major axis is aligned with the quantization field. We initialize the system to $|2,0\rangle$, with $\boldsymbol{B} = B_i\hat{b}_i$, and turn on the rf driving field with phase $\theta = 0$, to perform an on-resonance $\pi/2$ pulse, i.e., $\mathbf{\Omega}_1 T = (\pi/2)\hat{b}$, creating an equal superposition of the two clock states. Next we rotate the field adiabatically to $\mathbf{B} = B_f\hat{b}_f$, along the polarization plane, by an angle ϕ. We note that the magnetic field magnitude may vary as well. This will not affect our conclusions below.

As the magnetic field slowly rotates, the $|1,0\rangle$ and $|2,0\rangle$ clock states follow it adiabatically. They accumulate no dynamical phase, since their energy separation is magnetic field insensitive, and no Berry phase, since these are $m = 0$ states.

Next we perform an additional rf pulse with a rf phase θ for time T. Using Eq. (4), the probability to remain in the $|2,0\rangle$ state is

$$P_2 = \frac{1}{2} - \frac{|\cos(\theta)\cos(\phi) - \tilde{\Omega}\sin(\theta)\sin(\phi)|}{2\beta}\sin\left(\frac{\pi}{2}\beta\right), \qquad (6)$$

with β defined in Eq. (5). Assuming $\theta = (\pi/2)$, and a small rotation, this population becomes $P_2 = \frac{1}{2} - \frac{1}{2}\tilde{\Omega}\phi$, with quadratic corrections in ϕ. That is, P_2 is linear in the magnetic field rotation angle, and the polarization ellipse minor-to-major axes ratio is the sensitivity (slope). We expect this sensitivity to saturate at $\phi\tilde{\Omega} = 1$, as this is the value at which the leading-order approximation fails.

On the Bloch sphere spanned by the two clock states our method becomes intuitive. The two axes of the polarization ellipse are orthogonal to one another in quadrature; the first pulse acts as a τ^x rotation due to the major arm, rotating the state to the $-\hat{y}$ direction. In the absence of any magnetic field rotation, the $\pi/2$ phase-shifted second pulse acts as a τ^y rotation and does not affect the state. However, for a nonvanishing ϕ the state is rotated again by a τ^x operator, with a coupling strength equal to the magnetic field projection onto the ellipse's minor arm. If ϕ is large, it will overrotate the state, setting a limit on the measurement range.

Figure 2(a) shows the geometrical setup of the system. Figure 2(b) shows the probability to remain in the $|2,0\rangle$ state due to a rotation of the magnetic field ϕ, according to Eq. (6), with $\theta = (\pi/2)$. The sensitivity to rotations is the minor-to-major axes ratio $\tilde{\Omega}$, seen as the slope around $\phi = 0$. A trade-off between the sensitivity and measurement range is apparent, as a larger $\tilde{\Omega}$ reduces the distance between the curve maxima and minima.

In order to uncover the underlying phase difference acquired by the clock states, we make use of a Ramsey fringe measurement analogue. Instead of fixing the second pulse phase θ, we scan it and, according to Eq. (6), obtain a fringe. The fringe phase θ_f, i.e., the phase of the second pulse that maximizes the population in the $|2,0\rangle$ state, is given by

$$\theta_f = \pi - \mathrm{sgn}(\phi)\arccos[\cos(\phi)/\beta], \qquad (7)$$

with β defined in Eq. (5). For $\Omega_2 = \Omega_1$, we get $\beta = 1$, i.e., $\theta_f = \phi$, and in the limit $\Omega_2 \gg \Omega_1$, then θ_f converges to a step function around $\phi = 0$.

To compare our model's predictions to the experiment, we implemented the Ramsey sequence described above using a fixed elliptical microwave polarization with two main differences. Firstly, we added an additional π echo pulse in between the two $\pi/2$ pulses, in order to mitigate dephasing due to inhomogeneous trap-induced light shifts. Secondly, all pulse times were calibrated using the Rabi

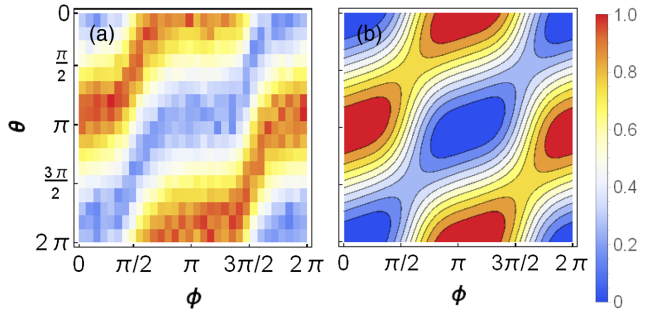

FIG. 3. Data and model of Ramsey sequence with field rotation. (a) Data, obtained by performing the Ramsey scheme as described in the main text. (b) Model according to Eq. (6), using $\tilde{\Omega} = 0.27$ in order to fit the data.

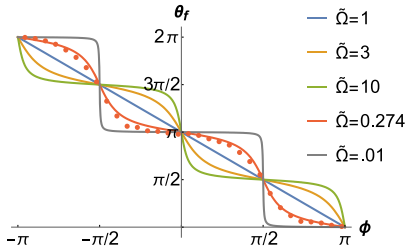

FIG. 4. Ramsey fringe phase of atomic clock states. Here the trade-off between sensitivity and measurement range is clearly seen as for $\tilde{\Omega} = 1$ (blue) the measurement range is 2π, yet by increasing it the slope around $\phi = 0$ increases dramatically but quickly saturates. We superimpose data (red points) obtained from the data shown in Fig. 3(a). Fitting these results to Eq. (7) we obtain $\tilde{\Omega} \approx 0.27$, which shows a good overlap with the theory (red solid). We also highlight the case $\tilde{\Omega} = 0.01$ (gray), demonstrating the topological phase of an open trajectory in parameter space [17].

flop data shown in Fig. 1, such that the fringe visibility remains constant at all rotation angles, without changing θ_f. By fitting the fringe phase to the expression in Eq. (7), we determined the minor-to-major ratio of our polarization ellipse to be $\tilde{\Omega} \approx 0.27$. Figure 3 shows the theoretical model in Eq. (6) and the measured data, which are in good agreement. The data clearly show that the clock state's phase can be manipulated via a magnetic field rotation.

Figure 4 shows the fringe phase for different minor-to-major axis ratios according to Eq. (7). The trade-off between sensitivity and measurement range is evident as larger minor-to-major ratios $\tilde{\Omega}$ result in a steeper change in θ_f; however, it also results in faster flattening of the slope and saturation of sensitivity. Using the experimental data shown in Fig. 3, we estimated the fringe phase for each field angle ϕ and added these as data points to Fig. 4 (red filled points) on top of the theoretical curve. As seen, the data and model are again in good agreement.

Figure 4 also shows the case $\tilde{\Omega} = 0.01$ (gray) which corresponds to an almost linear polarization along $\hat{b}$. This setting is obviously entirely insensitive to small field rotations; however it highlights the topological phase which does not require closing a path in parameter space [17], here seen as an abrupt and quantized π jump. This topological phase was verified experimentally in Ref. [22], where the magnetic field was reversed, and in Ref. [23], where rotations of the magnetic field by angles different than π were studied, showing a continuous loss of fringe visibility, but always a phase of either 0 or π. Here, by scanning the minor-to-major axes we interpolate between a continuous (blue) and abrupt (gray) phase change, generated by circular and linear polarizations, respectively.

These observations suggest a magnetic sensing method in which a small magnetic field $\boldsymbol{\delta}$ is sensed. Instead of rotating the quantization field direction between the two pulses, we simply ramp-down its magnitude adiabatically from B_i to B_f such that $B_i \gg B_f \gg \delta$. Assuming that $\boldsymbol{\delta} \| \hat{\Omega}_2$, i.e., it lies on the polarization plane and is perpendicular to $\hat{b}$, then when the quantization field is ramped-down the total magnetic field rotates such that $\phi = (\delta/B_f) + O[(\delta/B_f)^2]$. That is, the population change in Eq. (6) or the Ramsey phase in Eq. (7) becomes explicitly dependent on δ and linear in it in leading order, constituting a magnetic field measurement.

A unique property of this method is that the instantaneous magnetic field is sampled at the second pulse instant. Replacing the second pulse with a continuously modulated drive generates a spectral filter resulting in a spectrometer-like measurement of time-dependent magnetic fields [24].

We estimate the method's sensitivity. Ideally, the sensitivity is affected only by projection noise. We approximate the smallest change in δ that can be observed, $\Delta\delta$, using the Cramer-Rao bound [30,31],

$$\Delta\delta \approx \left[N \sum \mathcal{P}(x|\delta) \left(\frac{d \ln \mathcal{P}(x|\delta)}{d\delta} \right)^2 \right]^{-1/2}, \qquad (8)$$

where N is the number of independent identical measurements and the distribution $\mathcal{P}(x|\delta)$ is set by the probability to measure the state $|2,0\rangle$; i.e., it takes the value $x = 1$ with probability P_2, and $x = 0$ otherwise. Since we are concerned with small signals, Eq. (8) is evaluated at $\delta = 0$.

Using Eq. (6), with the second pulse phase set to $\theta = \frac{\pi}{2}$, Eq. (8) is evaluated to $\Delta\delta = B_f(\sqrt{N}\tilde{\Omega})^{-1}$. As expected, the sensitivity improves with more measurements and large minor-to-major ratio.

In theory our method's sensitivity is unlimited as both $\tilde{\Omega}^{-1}$ and B_f can be arbitrarily reduced. Practically, we expect the sensitivity to be determined by the clock subspace coherence time, τ_{clk}. Indeed, a more realistic analysis of Eq. (8), which takes into account population "leaks" out of the clock subspace, yields in leading order $\Delta\delta = (\hbar/\mu)(2\sqrt{2}/\sqrt{N}\tau_{\mathrm{clk}})$ [24].

This sensitivity is inversely dependent on the clock subspace coherence time, similarly to conventional Zeeman-Ramsey methods [32]. However, coherence times in clock subspaces are typically much longer than in Zeeman-split subspaces [33,34], implying that the proposed method may improve upon Zeeman-splitting-based magnetometry.

We note that the effect discussed here may be a source of shifts for atomic clocks, in which frequency stabilization is obtained by locking a local oscillator, e.g., a laser cavity, to an atomic transition [35]. In order to avoid shifts due magnetic field noise, a clock transition is driven with a linearly polarized field, using a Ramsey sequence. Any unwanted ellipticity of the driving field will couple to small rotations of the quantization axis $\Delta\phi$ that may occur between the two Ramsey pulses due to systematic effects. In leading order this will create an unwanted population difference between the clock states, $\Delta P = \frac{1}{2}\tilde{\Omega}\Delta\phi$, which will cause a systematic frequency shift of the clock.

In conclusion, we showed that atomic clock states can acquire a magnetic-field-dependent population difference and phase difference, that appear due to a rotation of the magnetic field, and measured it experimentally on a cloud of trapped ^{87}Rb atoms. We proposed a magnetic field sensing method that is sensitive to signals perpendicular to the quantization field.

This work was supported by the Crown Photonics Center, ICore-Israeli Excellence Center Circle of Light, the Israeli Science Foundation, the Israeli Ministry of Science Technology and Space, the Minerva Stiftung, and the European Research Council (Consolidator Grant No. 616919-Ionology).

*yotam.shapira@weizmann.ac.il

[1] M. Romalis and H. Dang, Atomic magnetometers for materials characterization, Mater. Today **14**, 258 (2011).
[2] M. N. Nabighian, V. J. S. Grauch, R. O. Hansen, T. R. Lafehr, Y. Li, J. W. Peirce, J. D. Phillips, and M. E. Ruder, The historical development of the magnetic method in exploration, Geophysics **70**, 33ND (2005).
[3] V. Mathe, F. Leveque, P. E. Mathe, C. Chevallier, and Y. Pons, Soil anomaly mapping using a caesium magnetometer: Limits in the low magnetic amplitude case, J. Appl. Geophys. **58**, 202 (2006).
[4] C. J. Berglund, L. R. Hunter, D. Krause, Jr., E. O. Prigge, M. S. Ronfeldt, and S. K. Lamoreaux, New Limits on Local Lorentz Invariance from Hg and Cs Magnetometers, Phys. Rev. Lett. **75**, 1879 (1995).
[5] I. Altarev *et al.*, Test of Lorentz Invariance with Spin Precession of Ultracold Neutrons, Phys. Rev. Lett. **103**, 081602 (2009).
[6] J. Lee, A. Almasi, and M. V. Romalis, Improved Limits on Spin-Mass Interactions, Phys. Rev. Lett. **120**, 161801 (2018).
[7] G. Bison, R. Wynands, and A. Weis, A laser-pumped magnetometer for the mapping of human cardiomagnetic fields, Appl. Phys. B **76**, 325 (2003).
[8] J. Belfi, G. Bevilacqua, V. Biancalana, S. Cartaleva, Y. Dancheva, and L. Moi, Cesium coherent population trapping magnetometer for cardiosignal detection in an unshielded environment, J. Opt. Soc. Am. B **24**, 2357 (2007).
[9] H. G. Dehmelt, Modulation of a light beam by precessing absorbing atoms, Phys. Rev. **105**, 1924 (1957).
[10] W. E. Bell and A. L. Bloom, Optical detection of magnetic resonance in alkali metal vapor, Phys. Rev. **107**, 1559 (1957).
[11] A. L. Bloom, Principles of operation of the rubidium vapor magnetometer, Appl. Opt. **1**, 61 (1962).
[12] J. Kitching, S. Knappe, and A. Donley, Atomic sensors—A review, IEEE Sens. J. **11**, 1749 (2011).
[13] C. L. Degen, F. Reinhard, and P. Cappellaro, Quantum sensing, Rev. Mod. Phys. **89**, 035002 (2017).
[14] L. Essen and J. V. L. Parry, An atomic standard of frequency and time interval: A cæsium resonator, Nature (London) **176**, 280 (1955).
[15] N. Yu, H. Dehmelt, and W. Nagourney, The 31S0-33P0 transition in the aluminum isotope ion 26A1+: A potentially superior passive laser frequency standard and spectrum analyzer, Proc. Natl. Acad. Sci. U.S.A. **89**, 7289 (1992).
[16] J. Terrien, News from the International Bureau of Weights and Measures, Metrologia **4**, 41 (1968).
[17] J. M. Robbins and M. V. Berry, A geometric phase for $m = 0$ spins, J. Phys. A: Math. Gen. **27**, L435 (1994).
[18] G. Breit and I. I. Rabi, Measurement of nuclear spin, Phys. Rev. **38**, 2082 (1931).
[19] D. A. Steck, Rubidium 87D line data, http://steck.us/alkalidata (2001).
[20] Y. Dallal, Spectroscopy of quasi-electrostatically trapped cold atoms, doctoral dissertation, Weizmann Institute of Science, Israel, 2014.
[21] Y. Dallal and R. Ozeri, Measurement of the Spin-Dipolar Part of the Tensor Polarizability of ^{87}Rb, Phys. Rev. Lett. **115**, 183001 (2015).
[22] K. Usami and M. Kozuma, Observation of a Topological and Parity-Dependent Phase of $m = 0$ Spin States, Phys. Rev. Lett. **99**, 140404 (2007).
[23] A. Takahashi, H. Imai, K. Numazaki, and A. Morinaga, Phase shift of an adiabatic rotating magnetic field in Ramsey atom interferometry for $m = 0$ sodium-atom spin states, Phys. Rev. A **80**, 050102(R) (2009).
[24] See Supplemental Material at http://link.aps.org/supplemental/10.1103/PhysRevLett.123.133204 for further derivation details, which includes Refs. [25–29].
[25] S. Kotler, N. Akerman, Y. Glickman, and R. Ozeri, Nonlinear Single-Spin Spectrum Analyzer, Phys. Rev. Lett. **110**, 110503 (2013).
[26] L. Landau, Zur theorie der energieubertragung. II, Phys. Z. Sowjetunion **2**, 46 (1932).
[27] C. Zener, Non-adiabatic crossing of energy levels, Proc. R. Soc. A **137**, 696 (1932).
[28] E. C. G. Stueckelberg, Theorie der unelastischen Stösse zwischen atomen, Helv. Phys. Acta **5**, 369 (1932).
[29] E. Shimshoni and A. Stern, Dephasing of interference in Landau-Zener transitions, Phys. Rev. B **47**, 9523 (1993).

[30] C. R. Rao, Information and the accuracy attainable in the estimation of statistical parameters, Bull. Calcutta Math. Soc. **37**, 81 (1945).

[31] H. Cramér, *Mathematical Methods of Statistics* (Princeton University Press, Princeton, NJ, 1946).

[32] D. Budker and M. Romalis, Optical magnetometry, Nat. Phys. **3**, 227 (2007).

[33] C. Langer, R. Ozeri, J. D. Jost, J. Chiaverini, B. DeMarco, A. Ben-Kish, R. B. Blakestad, J. Britton, D. B. Hume, W. M. Itano, D. Leibfried, R. Reichle, T. Rosenband, T. Schaetz, P. O. Schmidt, and D. J. Wineland, Long-Lived Qubit Memory Using Atomic Ions, Phys. Rev. Lett. **95**, 060502 (2005).

[34] G. Kleine Büning, J. Will, W. Ertmer, E. Rasel, J. Arlt, C. Klempt, F. Ramirez-Martinez, F. Piéchon, and P. Rosenbusch, Extended Coherence Time on the Clock Transition of Optically Trapped Rubidium, Phys. Rev. Lett. **106**, 240801 (2011).

[35] A. D. Ludlow, M. M. Boyd, and J. Ye, Optical atomic clocks, Rev. Mod. Phys. **87**, 637 (2015).